

2014

Network inefficiencies in autism spectrum disorder at 24 months

J R. Pruett

Washington University School of Medicine in St. Louis

K Botteron

Washington University School of Medicine in St. Louis

R McKinstry

Washington University School of Medicine in St. Louis

et al

Follow this and additional works at: http://digitalcommons.wustl.edu/open_access_pubs

Recommended Citation

Pruett, J R.; Botteron, K; McKinstry, R; and et al, "Network inefficiencies in autism spectrum disorder at 24 months." *Translational Psychiatry*.4, 1-11. (2014).

http://digitalcommons.wustl.edu/open_access_pubs/3776

This Open Access Publication is brought to you for free and open access by Digital Commons@Becker. It has been accepted for inclusion in Open Access Publications by an authorized administrator of Digital Commons@Becker. For more information, please contact engeszer@wustl.edu.

ORIGINAL ARTICLE

Network inefficiencies in autism spectrum disorder at 24 months

JD Lewis¹, AC Evans¹, JR Pruett², K Botteron², L Zwaigenbaum³, A Estes⁴, G Gerig⁵, L Collins¹, P Kostopoulos¹, R McKinstry², S Dager⁶, S Paterson⁷, RT Schultz⁷, M Styner^{8,9}, H Hazlett⁹ and J Piven⁹ for the IBIS network

Autism spectrum disorder (ASD) is a developmental disorder defined by behavioral symptoms that emerge during the first years of life. Associated with these symptoms are differences in the structure of a wide array of brain regions, and in the connectivity between these regions. However, the use of cohorts with large age variability and participants past the generally recognized age of onset of the defining behaviors means that many of the reported abnormalities may be a result of cascade effects of developmentally earlier deviations. This study assessed differences in connectivity in ASD at the age at which the defining behaviors first become clear. There were 113 24-month-old participants at high risk for ASD, 31 of whom were classified as ASD, and 23 typically developing 24-month-old participants at low risk for ASD. Utilizing diffusion data to obtain measures of the length and strength of connections between anatomical regions, we performed an analysis of network efficiency. Our results showed significantly decreased local and global efficiency over temporal, parietal and occipital lobes in high-risk infants classified as ASD, relative to both low- and high-risk infants not classified as ASD. The frontal lobes showed only a reduction in global efficiency in Broca's area. In addition, these same regions showed an inverse relation between efficiency and symptom severity across the high-risk infants. The results suggest delay or deficits in infants with ASD in the optimization of both local and global aspects of network structure in regions involved in processing auditory and visual stimuli, language and nonlinguistic social stimuli.

Translational Psychiatry (2014) 4, e388; doi:10.1038/tp.2014.24; published online 6 May 2014

INTRODUCTION

Autism spectrum disorder (ASD) is a developmental disorder defined by impairments in social communication and social interaction and a restricted repertoire of activities and interests.¹ Recent research has indicated that abnormalities in connectivity may underlie many of the behavioral symptoms. This research, however, is equivocal with respect to both the nature of connectivity abnormalities and the regions in which they occur, and currently provides little insight into their early developmental origins. Numerous studies have reported long-range under-connectivity in ASD,^{2–7} some have reported short-range over-connectivity accompanying long-range under-connectivity,^{8–13} and some have reported a less clearly divided mixture of over- and under-connectivity.^{14–16} Such connectivity abnormalities have been variously reported for virtually all pairs of brain regions.^{4–7,17–20}

This disparate set of findings reflects a variety of important methodological differences between studies, as well as small sample sizes and substantial etiologic and clinical heterogeneity. Prominent among the sources of variability is the wide variety of ages of the participants in these various studies. ASD is a developmental disorder involving complex networks comprising multiple spatially distributed brain regions which are developing in the context of a clearly altered growth trajectory. Children with ASD show abnormally rapid brain growth during the first years of

life,^{21–25} and abnormalities in the development of connectivity.²⁶ These brain-based abnormalities are likely to contribute to a developmental cascade of behavioral and neural abnormalities.²⁷ Thus, differences in findings of connectivity abnormalities in ASD may be owing to differences in the ages of the participants in various studies. The multitude of abnormalities in connectivity reported in adults with ASD, or even children with ASD, may tell us little about where in the brain these abnormalities first emerge. Identifying where connectivity abnormalities originate and how they develop has the potential to inform as to their cause, and to suggest more etiologically relevant paths to successful intervention. However, if we are to avoid confusing downstream developmental effects with source effects, this identification must be on the basis of data from individuals with ASD as early in development as possible, and with as little variation in age as possible.

Behavioral abnormalities may appear during the first year of life or early in the second year, but typically the characteristic symptoms of ASD necessary for classification only become stable by the end of the second year.^{28–31} If connectivity abnormalities underlie these symptoms of ASD, then differences in connectivity should also be present by the end of the second year of life, but downstream developmental effects should be minimal. Thus, to localize the early neural abnormalities in ASD, we assess connectivity at 24 months of age.

¹Montreal Neurological Institute, McGill University, Montreal, QC, Canada; ²Department of Psychiatry, Washington University School of Medicine, St Louis, MO, USA; ³Department of Pediatrics, University of Alberta, Edmonton, AB, Canada; ⁴Department of Speech and Hearing Sciences, University of Washington, Seattle, WA, USA; ⁵Scientific Computing and Imaging Institute, University of Utah, Salt Lake City, UT, USA; ⁶Department of Radiology, University of Washington, Seattle, WA, USA; ⁷Center for Autism Research, University of Pennsylvania, Philadelphia, PA, USA; ⁸Department of Computer Science, University of North Carolina, Chapel Hill, NC, USA and ⁹Carolina Institute for Developmental Disabilities, University of North Carolina, Chapel Hill, NC, USA. Correspondence: Dr JD Lewis, Montreal Neurological Institute, McGill University, 3801 University, WB208, Montreal, QC, Canada H3A 2B4.

E-mail: jlewis@bic.mni.mcgill.ca

Received 22 July 2013; revised 3 March 2014; accepted 8 March 2014

We utilize a whole-brain network analysis to assess white matter connectivity abnormalities in three groups of 24-month-olds: those with symptoms of ASD who also have an older sibling with ASD; those having an older sibling with ASD, but who are not themselves developing symptoms of ASD; and typically developing 24-month-olds with an older sibling and no first-degree relative with ASD or intellectual disability. Children with a sibling who has been diagnosed with ASD, but who do not receive a diagnosis themselves, often exhibit milder ASD symptoms.^{32,33} Thus this group might be expected to show a milder form of any connectivity abnormalities found in infants with significant symptoms of ASD.

A network analysis assesses connectivity on a whole-brain basis, rather than in terms of individual connections, thus providing measures which are relevant to overall brain organization.³⁴ Brain areas are treated as nodes in a graph; the connections between the brain areas constitute the edges of the graph. Properties of the overall network, or of subnetworks, associated with each participant can then be measured, and group differences assessed. This analytic approach has proved effective in characterizing differences in brain networks in a variety of clinical populations, including ASD.^{9,35}

Network analysis methods have evolved over the past 15 years, from straightforward applications of graph theory, which assess only network topology,³⁴ to more sophisticated approaches which take into account the spatial aspects of connectivity to assess the efficiency of information transfer within the network.^{36–39} Such approaches utilize measures of the length and strength of connections between all pairs of anatomical regions to estimate how efficiently information can be transferred between regions. This provides a way to assess the impact of abnormalities in spatial organization on communication, both across the brain and within local subnetworks. We use probabilistic tractography to estimate the strength of connectivity between all pairs of regions, and the length of the connections between regions. We then assess the group differences in local and global efficiency for each brain region, as well as the relation of efficiency to symptom severity, to determine where communication efficiency might be impaired in the brains of 24-month-olds with symptoms of ASD.

MATERIALS AND METHODS

Participants

The participants for this study were drawn from an ongoing multisite study of brain and behavioral development in infants at high risk for autism due to having an older sibling with ASD, known as the IBIS (Infant Brain Imaging Study), a study funded by the National Institute of Health via an Autism Center of Excellence grant. IBIS has enrolled and collected neuroimaging and behavioral data from these high-risk infants at 6, 12 and 24 months of age, with confirmation upon enrollment of the diagnosis

of their older sibling by medical record review and the Autism Diagnostic Interview. Data are also collected for infants deemed at relatively low risk for autism by virtue of having no first-degree relative with ASD or intellectual disability (as assessed by the Social Communication Questionnaire and the Family Interview for Genetic Studies), and an older sibling. A parent or legal guardian gave informed consent. Exclusionary criteria include the following conditions: (1) diagnosis or physical signs of genetic conditions/syndromes (for example, fragile X syndrome), (2) significant medical or neurological conditions affecting growth, development or cognition (for example, CNS infection, seizure disorder, congenital heart disease), (3) sensory impairments such as vision or hearing loss, (4) low birth weight (<2000) or prematurity (<36 weeks gestation), (5) evidence of significant perinatal brain injury or exposure to in-utero neurotoxins (for example, alcohol, selected prescription medications), (6) non-English speaking families, (7) contraindication for MRI (magnetic resonance imaging; for example, metal implants), (8) adopted children and (9) family history of first-degree relative with intellectual disability (not associated with ASD), psychosis, schizophrenia or bipolar disorder. The data were collected at four sites (University of North Carolina at Chapel Hill, University of Washington, Children's Hospital of Philadelphia, Washington University in St Louis); quality control and pre-processing were done at the University of Utah, the University of North Carolina at Chapel Hill and the Montreal Neurological Institute (McGill University), the Data Coordinating Center. The study was approved by the institutional review boards at all sites.

The subset of data used in the current study includes all 24-month data that passed quality control as of June 2012. These data divide according to whether the infants are high-risk or low-risk, and according to whether they showed ASD symptoms, as indexed by the Autism Diagnostic Observation Schedule (ADOS),⁴⁰ above the clinical cutoff for ASD. Participants were administered the ADOS at 24 months of age by trained researchers. Descriptives for the participants are shown in Table 1, with ADOS scores transformed to calibrated severity scores, as per Gotham *et al.*⁴¹ Note that Table 1 includes high-risk infants above the clinical cutoff for ASD (HR^{POS}), high-risk infants below the clinical cutoff for ASD (HR^{NEG}) and low-risk infants below the clinical cutoff for ASD (LR^{NEG}). There were three low-risk infants who received ADOS scores above the cutoff for ASD; their data were excluded. All other infants (a total of 136) were included in the analysis.

Imaging and image processing

MRI scans were done at each site on Siemens 3T TIM Trio scanners (Siemens Medical Systems, Erlangen, Germany) with 12-channel head coils. Intra- and inter-site reliability was verified.⁴² Data were collected while infants were naturally sleeping. Three types of images were acquired: (1) T_1 -weighted images using a 3D MPRAGE sequence (resolution = $1.0 \times 1.0 \times 1.0$ mm; TE = 3.16 ms; TR = 2400 ms; matrix = 224×256); (2) T_2 -weighted images using a 3D FSE sequence (resolution = $1.0 \times 1.0 \times 1.0$ mm; TE = 499 ms; TR = 3200 ms; matrix = 256×256); and (3) diffusion-weighted images using a 2D echo planar sequence (resolution = $2.0 \times 2.0 \times 2.0$; TE = 102 ms; TR = 12 800 ms; directions = 25; b-values: unique values evenly distributed between 0 and 1000 s mm^{-2}). Data were quality controlled, starting at the MRI console; where motion artifacts were observed, the scan sequence was repeated to possibly acquire artifact free data.

The T_1 - and T_2 -weighted images were subjected to manual quality control, and corrected for geometric distortion.⁴³ The diffusion-weighted images were cleaned of motion and other artifacts using DTIPrep,⁴⁴ which corrects artifacts where possible, and excludes directions from the data when correction is not possible. Only data sets with acceptable T_1 -, T_2 - and diffusion-weighted images were included in the analysis.

The distortion-corrected T_1 - and T_2 -volumes were then processed with CIVET, a fully automated structural image analysis pipeline developed at the Montreal Neurological Institute. CIVET corrects intensity nonuniformities using N3;⁴⁵ aligns the input volumes to the Talairach-like ICBM-152-nl template;⁴⁶ classifies the image into white matter, gray matter, cerebrospinal fluid and background;^{47,48} extracts the white matter and pial surfaces;⁴⁹ and warps these to a common surface template.⁵⁰ The CIVET results were used to construct the seed, stop and target masks for use with FSL's probtrackx.⁵¹ Seed masks specify the voxels from which tracts propagate; seed masks were the entire white matter. Stop masks specify where tract propagation is halted; stop masks were the voxels on the boundary of the white matter. Target masks determine the interpretation of tracts; target masks were the cortical labels of the automatic anatomical

Table 1. Sample characteristics

Age (months)	HR ^{POS}			HR ^{NEG}			LR ^{NEG}		
	N	Mean	s.d.	N	Mean	s.d.	N	Mean	s.d.
Male	24	24.85	0.64	51	24.76	0.74	12	24.62	0.70
Female	7	25.05	0.82	31	24.72	1.11	11	24.45	0.54
ADOS severity									
Male	—	6.13	1.60	—	1.36	0.70	—	1.33	0.65
Female	—	5.14	1.86	—	1.29	0.64	—	1.22	0.67

Abbreviations: HR^{POS}, high-risk infants with ADOS scores above the clinical cutoff for ASD; HR^{NEG}, high-risk infants with ADOS scores below the clinical cutoff for ASD; LR^{NEG}, low-risk infants with ADOS scores below the clinical cutoff for ASD.

labelling (AAL) atlas,⁵² a parcellation based on anatomical landmarks, predominately sulci, defined on the common surface template.⁵³

The diffusion-weighted images were unwarped via nonlinear registration to the distortion-corrected T_2 -volume, and then preprocessed for probabilistic tractography with FSL's bedpostx.⁵¹ The default parameters for bedpostx were used: a maximum of two fibers per voxel, a multiplicative factor of 1 on the prior for the second fiber and a burn-in of 1000. The unwarped diffusion volumes were also affine registered to the T_1 -volumes using FSL's flirt⁵⁴ to provide the mapping from the seed, stop and target masks to the diffusion space. Probabilistic tractography, utilizing FSL's probtrackx was then seeded twice from 10 000 random locations within each voxel of the seed masks: with distance-bias correction^{51,55} to generate the number of tracts connecting voxels in the target mask, and without distance-bias correction to generate the physical lengths of those tracts. These results were then compiled for each AAL region, generating undirected matrices of the total number of connections between each pair of AAL regions, and the mean physical length of those connections. The total number of connections between each pair of AAL regions divided by the average surface area of the two AAL regions is referred to as connection 'strength'.

Analysis

Network analyses investigate the organization of sets of connections, rather than considering the connections independently. The metric utilized here is efficiency, as defined by Latora and Marchiori.^{36,37} Network efficiency is the capacity to exchange information across a network. Latora and Marchiori³⁶ defined the efficiency ϵ_{ij} in the communication between nodes i and j to be inversely proportional to the shortest path length d_{ij} between nodes i and j . They take the shortest path length d_{ij} to be the smallest sum of the physical distances throughout all of the possible paths from i to j in the graph. The efficiency of a network, G , is then

$$E(G) = \frac{\sum_{i \neq j \in G} \epsilon_{ij}}{N(N-1)} = \frac{1}{N(N-1)} \sum_{i \neq j \in G} \frac{1}{d_{ij}}$$

where N is the number of nodes in the network graph G ; ϵ_{ij} is the efficiency of the connection between nodes i and j ; and d_{ij} is the length of the shortest path, in terms of physical distances, between nodes i and j . This measure is normalized by $E(G_{IDEAL})$, the fully connected network. This formulation is importantly different from most graph theoretic measures, which assess only the topological properties of networks,^{34,38,56} the measures of efficiency take into account the physical distances involved in information transfer, and so presumably relate more closely to the neurobiological substrates.

Latora and Marchiori³⁶ apply this formulation to both the entire network, which they refer to as global efficiency, and to the subnetworks of the immediate neighbors of each node; they define local efficiency as the mean of $E(G_i)$, for all nodes i , where G_i is the subgraph of all the neighbors of node i . These definitions give a single measure of local efficiency and of global efficiency for the entire network. But, the definitions can be reformulated to provide measures of efficiency for each node, or for collections of nodes. Achard and Bullmore³⁸ define nodal efficiency, which we will refer to as nodal global efficiency, as the inverse of the harmonic mean of the minimum path length between a node, i , and all other nodes in the network. Utilizing the physical distances, as per Latora and Marchiori,³⁶ the nodal global efficiency of node i is thus

$$E_{\text{nodalglobal}}(G, i) = \frac{\sum_{j \in G, j \neq i} \epsilon_{ij}}{(N-1)} = \frac{1}{(N-1)} \sum_{j \in G, j \neq i} \frac{1}{d_{ij}}$$

where N is the number of nodes in the network graph G ; ϵ_{ij} is the efficiency of the connection between nodes i and j ; and d_{ij} is the length of the shortest path, in terms of tractography-based measures of physical distances, between nodes i and j . The definition of local efficiency can likewise be parsed to provide a measure of nodal local efficiency; recall that the local efficiency of a network is the mean of $E(G_i)$, for all nodes i , where G_i is the subgraph of all the neighbors of node i . Thus the nodal local efficiency of node i is simply

$$E_{\text{nodallocal}}(G, i) = \frac{\sum_{j \neq k \in G_i} \epsilon_{jk}}{N_{G_i}(N_{G_i} - 1)} = \frac{1}{N_{G_i}(N_{G_i} - 1)} \sum_{j \neq k \in G_i} \frac{1}{d_{jk}}$$

where N_{G_i} is the number of nodes in the subgraph G_i consisting of all of the neighbors of i ; ϵ_{jk} is the efficiency of the connection between nodes j and k ; and d_{jk} is the length of the shortest path, in terms of tractography-based measures of physical distances, between nodes j and k .

These definitions treat connections in a binarized fashion. But the strengths of the connections in the brain are critical to an accurate assessment of its efficiency.⁵⁷ We thus utilize a version of these measures that does not discard information about connection strength by thresholding, but rather incorporates connection strengths. On the basis of Rubinov and Sporns,⁵⁶ we define the weighted distance between nodes i and j as

$$d_{ij}^w = \frac{d_{ij}}{w_{ij}}$$

where d_{ij} is the length of the shortest path, in terms of tractography-based measures of physical distances, between nodes i and j ; and w_{ij} is the connection strength between nodes i and j . The length of the shortest path in terms of weighted distances is thus related to the travel time along the path, decreasing with the strengths of the connections involved, and increasing with the tractography-based measures of the physical distances involved. Our weighted formulations of nodal global efficiency and nodal local efficiency, also based on Rubinov and Sporns,⁵⁶ are

$$E_{\text{nodalglobal}}^{\text{weighted}}(G, i) = \frac{1}{(N-1)} \sum_{j \in G, j \neq i} \left(d_{ij}^w\right)^{-1}$$

where N is the number of nodes in the network graph G ; and d_{ij}^w is the shortest path, in terms of weighted distance, between nodes i and j ; and

$$E_{\text{nodallocal}}^{\text{weighted}}(G, i) = \frac{1}{N_{G_i}(N_{G_i} - 1)} \sum_{j \neq k \in G_i} \left(\left(d_{jk}^w\right)^{-1} w_{ij} w_{ik} \right)^{1/3}$$

where N_{G_i} is the number of nodes in the subgraph G_i consisting of all of the neighbors of i ; d_{jk}^w is the shortest path, in terms of weighted distance, between nodes j and k ; and w_{ij} and w_{ik} are the connection strengths between nodes i and j , and i and k , respectively. As per Latora and Marchiori,³⁶ these measures are normalized by considering the fully connected network.

Group differences in nodal local efficiency and nodal global efficiency were assessed via statistical linear models, controlling for age, sex and site, in models which included all three groups. To determine the extent to which any group differences in network structure were driven by individual behavioral differences, we also assessed the relation between the measures of network efficiency and the ADOS-based calibrated severity scores⁴¹ within the high-risk infants, controlling for age, sex and site. To gain further insight into the proper interpretation of any group differences in nodal local efficiency and nodal global efficiency, a *post hoc* analysis was performed to assess group differences in three additional properties of the networks associated with each node: the strengths of the connections comprising the paths contributing to the efficiency measures; the tract-based lengths of those paths; and the number of edges in those paths. For each of these measures, the contribution associated with the path between nodes j and k to the nodal local measure at node i is determined by the connection strength between nodes i and j , and i and k , exactly as in the case of nodal local efficiency. The nodal global measures at node i are the mean of the measures associated with the paths contributing to nodal global efficiency at node i .

RESULTS

Relative to LR^{NEG} infants, the HR^{POS} infants showed reductions in nodal local efficiency bilaterally in the temporal and occipital lobes in inferior and medial regions, and predominately in the right hemisphere for lateral regions, extending to the supramarginal gyrus (Figure 1, top left). Relative to LR^{NEG} infants, the HR^{POS} infants showed reductions in nodal global efficiency in bilateral temporal and occipital regions, extending in the right hemisphere to the angular and supramarginal gyri; the left hemisphere reductions include the pars triangularis and orbital gyrus. (Figure 1, bottom left). There were no significant increases in either nodal local or nodal global efficiency in the HR^{POS} infants relative to the LR^{NEG} infants. The group differences in nodal local efficiency for HR^{POS} compared with HR^{NEG} infants are similar to those in the comparison of the HR^{POS} and LR^{NEG} infants, but left lateralized and less extensive. Relative to the HR^{NEG} infants, the HR^{POS} infants showed reductions in nodal local efficiency over the left hemisphere temporal and occipital lobes, and the precuneus; the right hemisphere differences are mostly nonsignificant

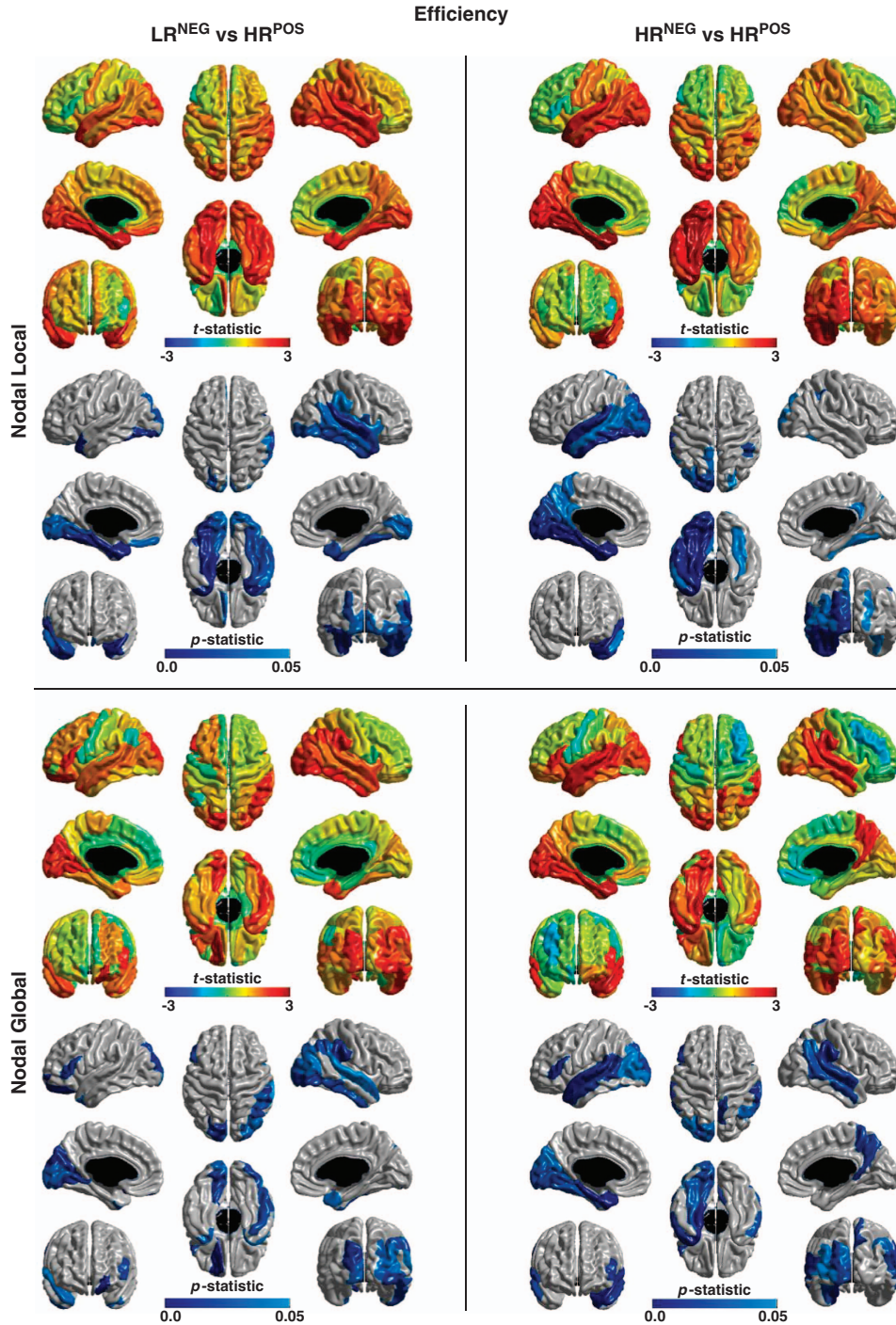


Figure 1. The comparison of nodal local and nodal global efficiency for LR^{NEG} versus HR^{POS} infants, and for HR^{NEG} versus HR^{POS} infants, in a model with all three groups, controlling for age, sex and site. The top half of the figure shows the *t*- and *p*-statistic for the comparison of nodal local efficiency in each region of the AAL atlas; the bottom half of the figure shows the *t*- and *p*-statistic for the comparison of nodal global efficiency. The left column shows the comparisons for LR^{NEG} versus HR^{POS} infants; the right column for HR^{NEG} versus HR^{POS} infants. A positive *t*-statistic represents a relative reduction in efficiency in HR^{POS} infants. No regions show significantly increased nodal local or global efficiency in HR^{POS} infants. Significant reductions in nodal local efficiency in HR^{POS} compared with LR^{NEG} infants are seen bilaterally in the temporal and occipital lobes in inferior and medial regions, and predominantly in the right hemisphere for lateral regions, extending to the supramarginal gyrus. Significant reductions in nodal local efficiency in HR^{POS} compared with HR^{NEG} infants are seen in the left temporal and occipital lobes, extending into the precuneus, and in several posterior regions in the right hemisphere. Significant reductions in nodal global efficiency in HR^{POS} infants compared with LR^{NEG} infants are seen bilaterally in the temporal and occipital lobes, extending in the right hemisphere to the angular and supramarginal gyri. The left pars triangularis and medial orbital gyrus also show reduced nodal global efficiency. Significant reductions in nodal global efficiency in HR^{POS} infants compared with HR^{NEG} infants are seen in bilateral temporal lobes, extending in the left hemisphere to the occipital cortex, and in the right hemisphere to the angular and supramarginal gyri. The left hemisphere reductions include the medial temporal and occipital regions, and the pars triangularis. The right hemisphere reductions include the precuneus. Note that in all cases the reductions are predominately posterior. HR^{NEG}, high-risk infants with ADOS scores below the clinical cutoff for ASD; HR^{POS}, high-risk infants with ADOS scores above the clinical cutoff for ASD; LR^{NEG}, low-risk infants with ADOS scores below the clinical cutoff for ASD.

(Figure 1, top right). The group differences in nodal global efficiency for HR^{POS} compared with HR^{NEG} infants are also similar to those in the comparison of the HR^{POS} and LR^{NEG} infants, but with greater reductions in the left hemisphere. Significant reductions in HR^{POS} infants compared with HR^{NEG} infants are seen in bilateral temporal lobes, extending in the left hemisphere to the occipital cortex, and in the right hemisphere to the angular and supramarginal gyri. The left hemisphere reductions include the pars triangularis. The right hemisphere reductions include the precuneus (Figure 1, bottom right). There were no significant increases in either nodal local or global efficiency in the HR^{POS} infants relative to the HR^{NEG} infants. The HR^{NEG} and LR^{NEG} infants showed no group differences; but note that the results are spatially graded: HR^{POS} infants showed more extensive reductions relative to LR^{NEG} infants than to the HR^{NEG} infants. Also note that in all the cases the reductions are predominately posterior.

The relationship between the measures of network efficiency and the ADOS-based calibrated severity scores within the high-risk infants are similar to the group differences in efficiency for the two subgroups of the high-risk infants, that is, the HR^{POS} compared with HR^{NEG} infants. There is a significant inverse relation of severity to nodal local efficiency in the left temporal and occipital lobes (Figure 2, top). This inverse relation is significant in the lingual gyrus, and throughout the temporal lobe, with the exception of the middle temporal gyrus. There is a significant inverse relation of severity to nodal global efficiency in the left temporal lobe and in Broca's area (Figure 2, bottom). This inverse relation is significant throughout the temporal lobe, with the exception of the inferior temporal gyrus. Note that where there is a significant relation between efficiency and severity, in all cases this is an inverse relation, thus greater symptom severity corresponds to lesser efficiency. Also note that, as with the group differences, this inverse relation is only present in posterior regions, and in Broca's area for nodal global efficiency.

The *post hoc* analyses of the group differences in the strengths of the connections comprising the paths contributing to the efficiency measures, the tract-based lengths of those paths, and the number of edges in those paths indicates that these results stem from both weaker connections and abnormalities in network structure. The reductions in nodal local and nodal global efficiency in HR^{POS} infants are partially paralleled by reductions in connection strength in the paths involved. Relative to LR^{NEG} infants, the HR^{POS} infants showed reductions in nodal local connection strength bilaterally in the temporal, parietal and occipital lobes, and in the left medial orbital gyrus (Figure 3, top left). Relative to LR^{NEG} infants, the HR^{POS} infants showed reductions in nodal global connection strength in the right inferior temporal and occipital lobes (Figure 3, bottom left). There

were no significant increases in either nodal local or nodal global connection strength in the HR^{POS} infants relative to the LR^{NEG} infants. Relative to HR^{NEG} infants, the HR^{POS} infants showed reductions in nodal local connection strength in bilateral temporal and parietal lobes, the right precuneus and gyrus rectus, and the left pars triangularis and medial orbital gyrus (Figure 3, top right). Relative to HR^{NEG} infants, the HR^{POS} infants showed reductions in

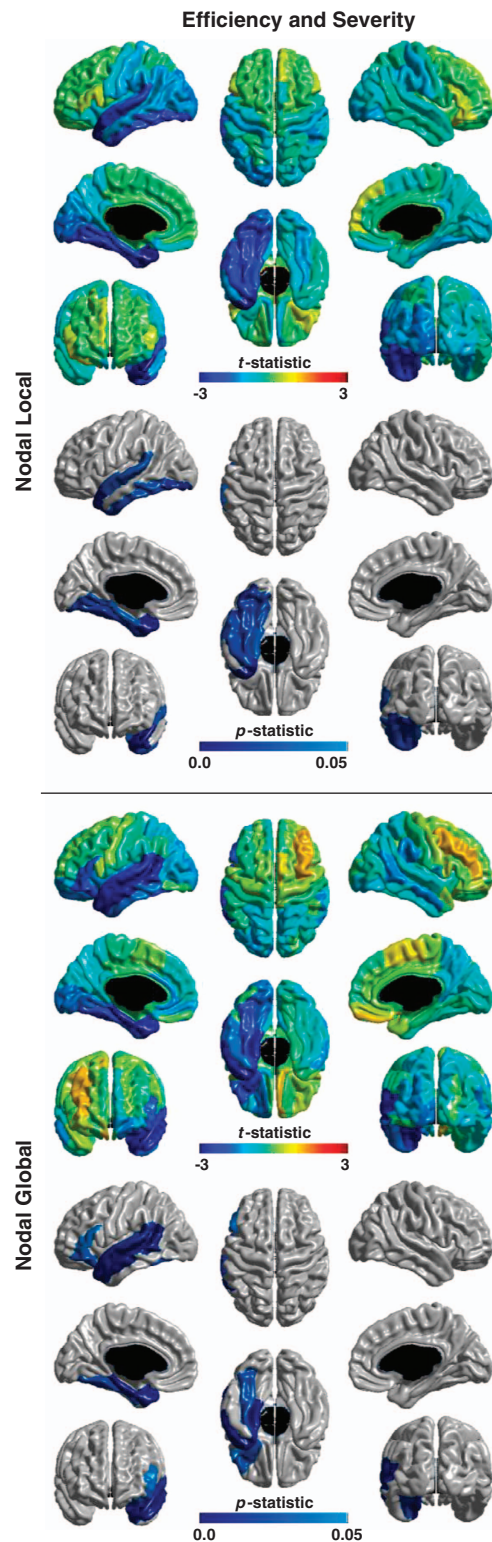


Figure 2. The relation of ADOS-based calibrated severity to network efficiency in the high-risk infants, controlling for age, sex and site. The top half of the figure shows the *t*- and *p*-statistic for the relation of severity and nodal local efficiency in each region of the AAL atlas; the bottom half of the figure shows the *t*- and *p*-statistic for the relation of severity and nodal global efficiency. A negative *t*-statistic represents an inverse relation between severity and efficiency, that is, greater symptom severity corresponds to lesser efficiency. There is a significant inverse relation of severity to nodal local efficiency in the left lingual gyrus, and throughout the left temporal lobe, with the exception of the middle temporal gyrus. There is a significant inverse relation of severity to nodal global efficiency in Broca's area, and throughout the left temporal lobe, with the exception of the inferior temporal gyrus. Note that all significant relations are inverse relations, and that these are only present in the left temporal and occipital lobes, and in Broca's area for nodal global efficiency. AAL, automatic anatomical labelling; ADOS, Autism Diagnostic Observation Schedule.

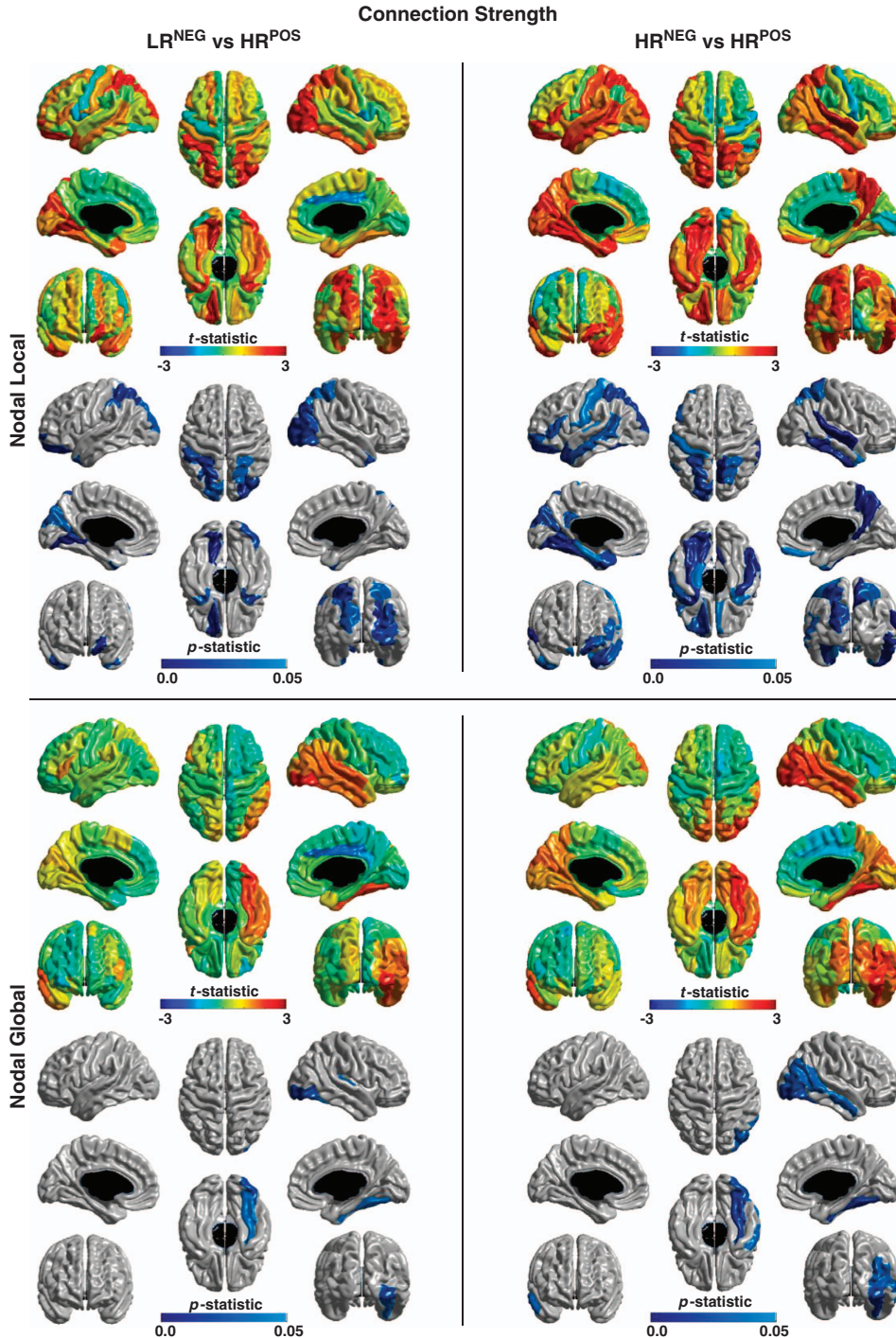


Figure 3. The comparison of the mean connection strength in the paths comprising the measures of nodal local and nodal global efficiency for LR^{NEG} versus HR^{POS} infants, and for HR^{NEG} versus HR^{POS} infants, in a model with all three groups, controlling for age, sex and site. The top half of the figure shows the *t*- and *p*-statistic for the comparison of nodal local connection strength in each region of the AAL atlas; the bottom half of the figure shows the *t*- and *p*-statistic for the comparison of nodal global connection strength. The left column shows the comparisons for LR^{NEG} versus HR^{POS} infants; the right column for HR^{NEG} versus HR^{POS} infants. A positive *t*-statistic represents a relative reduction in connection strength in HR^{POS} infants. No regions show significantly increased connection strength in HR^{POS} infants. Significant reductions in nodal local connection strength in HR^{POS} compared with LR^{NEG} infants are seen bilaterally in the temporal, parietal and occipital lobes, and in the left medial orbital gyrus. Significant reductions in nodal local connection strength in HR^{POS} compared with HR^{NEG} infants are seen in bilateral temporal and parietal lobes, the right precuneus and gyrus rectus, and the left pars triangularis and medial orbital gyrus. Significant reductions in nodal global connection strength in HR^{POS} infants compared with LR^{NEG} infants are seen in the right fusiform gyrus and inferior occipital lobe. Significant reductions in nodal global connection strength in HR^{POS} infants compared with HR^{NEG} infants are seen in the right temporal and occipital lobes. Note that, as with efficiency, in all cases the reductions are predominately posterior. HR^{NEG}, high-risk infants with ADOS scores below the clinical cutoff for ASD; HR^{POS}, high-risk infants with ADOS scores above the clinical cutoff for ASD; LR^{NEG}, low-risk infants with ADOS scores below the clinical cutoff for ASD.

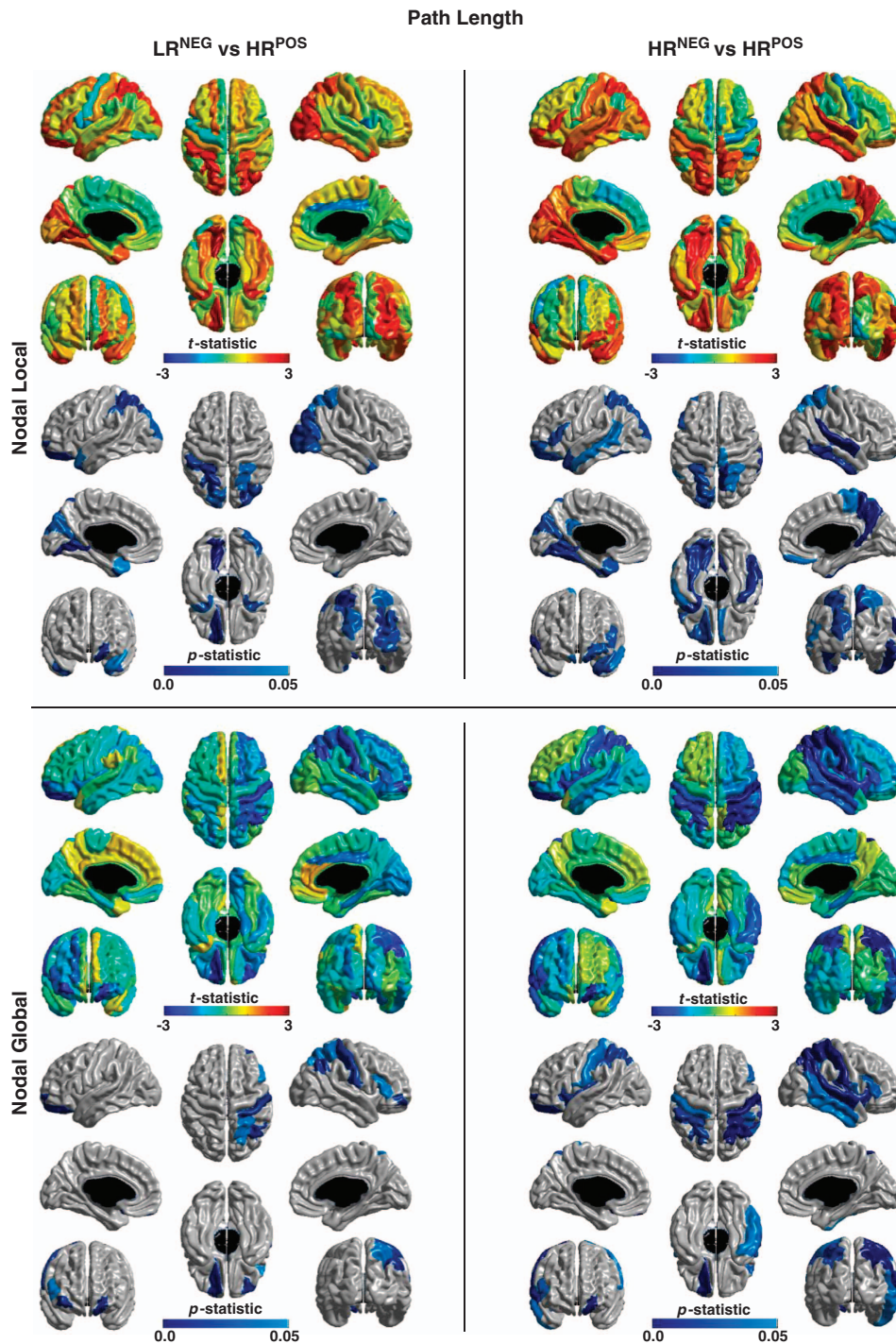


Figure 4. The comparison of the mean length of the paths comprising the measures of nodal local and nodal global efficiency for LR^{NEG} versus HR^{POS} infants, and for HR^{NEG} versus HR^{POS} infants, in a model with all three groups, controlling for age, sex and site. The top half of the figure shows the *t*- and *p*-statistic for the comparison of nodal local mean path length in each region of the AAL atlas; the bottom half of the figure shows the *t*- and *p*-statistic for the comparison of nodal global mean path length. The left column shows the comparisons for LR^{NEG} versus HR^{POS} infants; the right column for HR^{NEG} versus HR^{POS} infants. A positive *t*-statistic represents a relative reduction in mean path length in HR^{POS} infants. Significant reductions in nodal local mean path length in HR^{POS} compared with LR^{NEG} infants are seen bilaterally in the temporal, parietal and occipital lobes, and in the left medial orbital gyrus. Significant reductions in nodal local mean path length in HR^{POS} compared with HR^{NEG} infants are seen in bilateral temporal, parietal and occipital lobes, the right precuneus, paracentral lobule and gyrus rectus, and the left pars triangularis and medial orbital gyrus. No regions show significantly increased nodal local mean path length in HR^{POS} infants relative to either LR^{NEG} or HR^{NEG} infants. Significant increases in nodal global mean path length in HR^{POS} infants compared with LR^{NEG} infants are seen in the right parietal lobe, the right pars triangularis and the left medial orbital gyrus. Significant increases in nodal global mean path length in HR^{POS} infants compared with HR^{NEG} infants are seen bilaterally in the parietal lobe, and in the right temporal lobe and left medial orbital gyrus. No regions show significantly decreased nodal global mean path length in HR^{POS} infants relative to either LR^{NEG} or HR^{NEG} infants. Note that, as with efficiency, in all cases the group differences are predominately posterior. AAL, automatic anatomical labelling; HR^{NEG}, high-risk infants with ADOS scores below the clinical cutoff for ASD; HR^{POS}, high-risk infants with ADOS scores above the clinical cutoff for ASD; LR^{NEG}, low-risk infants with ADOS scores below the clinical cutoff for ASD.

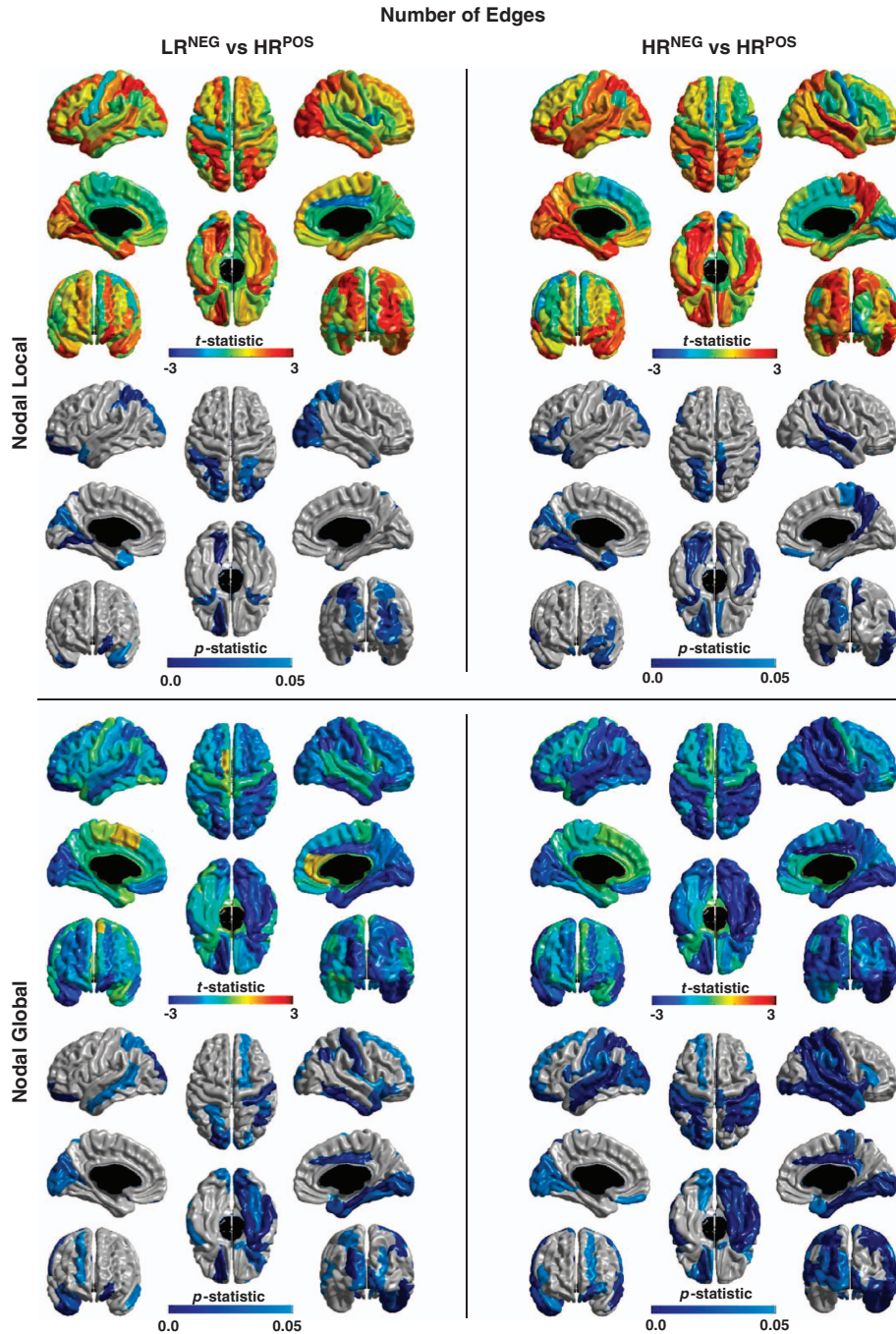


Figure 5. The comparison of the mean number of edges in the paths comprising the measures of nodal local and nodal global efficiency for LR^{NEG} versus HR^{POS} infants, and for HR^{NEG} versus HR^{POS} infants, in a model with all three groups, controlling for age, sex and site. The top half of the figure shows the *t*- and *p*-statistic for the comparison of nodal local mean number of edges in each region of the AAL atlas; the bottom half of the figure shows the *t*- and *p*-statistic for the comparison of nodal global mean number of edges. The left column shows the comparisons for LR^{NEG} versus HR^{POS} infants; the right column for HR^{NEG} versus HR^{POS} infants. A positive *t*-statistic represents a relative reduction in mean number of edges in HR^{POS} infants. Significant reductions in nodal local mean number of edges in HR^{POS} compared with LR^{NEG} infants are seen bilaterally in the temporal, parietal and occipital lobes, and in the left medial orbital gyrus. Significant reductions in nodal local mean number of edges in HR^{POS} compared with HR^{NEG} infants are seen in bilateral temporal and parietal lobes, the right precuneus, paracentral lobule, and gyrus rectus, and the left cuneus, pars triangularis and medial orbital gyrus. No regions show significantly increased nodal local mean number of edges in HR^{POS} infants relative to either LR^{NEG} or HR^{NEG} infants. Significant increases in nodal global mean number of edges in HR^{POS} infants compared with LR^{NEG} infants are seen in bilateral temporal, parietal and occipital lobes, the right superior frontal gyrus, and the left medial orbital gyrus. Significant increases in nodal global mean number of edges in HR^{POS} infants compared with HR^{NEG} infants are seen in bilateral temporal, parietal and occipital lobes, the left superior frontal gyrus, medial orbital gyrus, gyrus rectus and pars opercularis, and the right pars triangularis, paracentral lobule and cingulate cortex. No regions show significantly decreased nodal global mean number of edges in HR^{POS} infants relative to either LR^{NEG} or HR^{NEG} infants. Note that, as with efficiency, in all cases the group differences are predominately posterior. HR^{NEG}, high-risk infants with ADOS scores below the clinical cutoff for ASD; HR^{POS}, high-risk infants with ADOS scores above the clinical cutoff for ASD; LR^{NEG}, low-risk infants with ADOS scores below the clinical cutoff for ASD.

nodal global connection strength in the right temporal and occipital lobes (Figure 3, bottom right). There were no significant increases in either nodal local or nodal global connection strength in the HR^{POS} infants relative to the HR^{NEG} infants. Note that, as with efficiency, in all cases the reductions are predominately posterior.

The reductions in nodal local and nodal global efficiency in HR^{POS} infants appear to be not only the result of weaker connections, but also abnormalities in network structure. Relative to LR^{NEG} infants, the HR^{POS} infants showed significantly reduced nodal local mean path length in bilateral temporal, parietal and occipital lobes, and the left medial orbital gyrus (Figure 4, top left). The fact that this group difference is almost identical to the group difference in nodal local mean number of edges (Figure 5, top left) indicates that these networks have reduced spatial extent. Relative to LR^{NEG} infants, the HR^{POS} infants showed significantly increased nodal global mean path length in the right parietal lobe, the right pars triangularis, and the left medial orbital gyrus (Figure 4, bottom left). The comparison of nodal global mean number of edges also shows increases in HR^{POS} infants in posterior regions, more bilaterally in this case, as well as in the right lateral orbital and superior frontal gyri, and the left medial orbital gyrus (Figure 5, bottom left). Thus, relative to LR^{NEG} infants, HR^{POS} infants have on average longer, less direct paths connecting a node with other brain regions. Relative to HR^{NEG} infants, the HR^{POS} infants showed significantly reduced nodal local mean path length in bilateral temporal and parietal lobes, the left occipital lobe, pars triangularis and medial orbital gyrus, and the right precuneus, paracentral lobule, and gyrus rectus (Figure 4, top right). Again, this group difference is exactly mirrored by the group difference in nodal local mean number of edges (Figure 5, top right) indicating that nodal local networks have reduced spatial extent in HR^{POS} infants. Relative to HR^{NEG} infants, the HR^{POS} infants showed significantly increased nodal global mean path length in bilateral parietal lobes, the right temporal lobe and pars triangularis, and the left medial orbital gyrus (Figure 4, bottom right). The comparison of nodal global mean number of edges shows increases in HR^{POS} infants in bilateral temporal, parietal and occipital lobes, as well as in the left medial orbital and superior frontal gyri, the left medial orbital gyrus and pars orbitalis, and the right pars triangularis, paracentral lobule and cingulate gyrus (Figure 5, bottom right). Thus, relative to HR^{NEG} infants, HR^{POS} infants have on average longer, less direct paths connecting a node with other brain regions.

DISCUSSION

Network efficiency measures from diffusion-based probabilistic tractography were significantly reduced, predominately in posterior brain regions, in HR^{POS} infants relative to both LR^{NEG} and HR^{NEG} infants at 24 months of age, and were inversely related to ASD symptom severity. HR^{POS} infants showed reduced nodal global efficiency, relative to both LR^{NEG} and HR^{NEG} infants, over the right superior temporal, angular and supramarginal gyri, and the left pars triangularis, cuneus and lingual gyrus. HR^{POS} infants showed reduced nodal local efficiency, relative to both LR^{NEG} and HR^{NEG} infants, over bilateral inferior temporal gyri, the left fusiform, parahippocampal and lingual gyri, temporal pole, and medial occipital cortex. Relative to the HR^{NEG} infants, the HR^{POS} infants showed more bilateral reductions in nodal global efficiency and more left lateralized reductions in nodal local efficiency. In either case, the abnormalities were concentrated in posterior regions; the frontal lobes showed no differences, with the exception of the anterior portion of Broca's area. The significant differences in the HR^{POS} infants were all reductions in efficiency. Further, both nodal local and nodal global efficiency showed an inverse relation to ASD symptoms, as indexed by ADOS-based calibrated severity scores within the high-risk infants, over left temporal and occipital

regions, and in Broca's area for nodal global efficiency. The regions implicated are involved in processing auditory and visual stimuli, language and nonlinguistic social stimuli, for example, faces, and in memory, all of which show abnormalities in ASD.^{58–65}

These results align with a number of findings in infant siblings of children with autism, and older children with ASD. Infant siblings of children with autism have been shown to have atypicalities in both visual and auditory processing,^{66–69} as well as an inability to integrate audio-visual information;⁷⁰ in addition, connections between the bilateral occipital lobes have been implicated in relation to visual orienting in infants who go on to develop symptoms of ASD.⁶⁶ Studies in toddlers with symptoms of ASD have shown reduced correlation in functional data between bilateral superior temporal gyri,⁷¹ and reduced activation in response to speech stimuli in the left superior temporal gyrus.⁷² Slightly older children with ASD show reduced correlation in functional data between bilateral inferior frontal gyri.⁷¹ Hypoperfusion in bilateral temporal and temporal-parietal regions has also been reported in older children with ASD,^{73–76} and a negative relation between cerebral blood flow and autism severity in the left superior temporal gyrus.⁷⁷ Structural abnormalities in older children with autism include localized gray matter reductions within ventral and superior temporal cortical areas, as well as parietal areas.⁷⁸

Frontal cortico-cortical connectivity abnormalities, which are well documented in adolescents and adults with ASD,^{7,79,80} presumably emerge over development together with the behavioral abnormalities with which they are associated. In children, the frontal lobes show few network abnormalities, whereas posterior regions show widespread abnormalities both locally and globally.^{9,35}

The reductions in nodal local and nodal global efficiency shown here for the HR^{POS} infants correspond to a number of organizational differences. The paths underlying these reductions in efficiency were shown to be comprised of generally weaker connections, that is, fewer, smaller or less well-myelinated fibers. In the case of nodal global efficiency the paths involved were also shown to be on average physically longer and more indirect, that is, to pass through more intermediary nodes. In the case of nodal local efficiency the paths involved were comprised of weaker, but generally physically shorter and more direct paths in the HR^{POS} infants. But as the degree to which a node is a neighbor of another is determined by the strength of the direct connection between them, and the nodal global connection strength is decreased in the HR^{POS} infants, the physically shorter and more direct paths in the HR^{POS} infants represents reduced spatial extent of the nodal local networks. Thus, the reduction in nodal local efficiency in the HR^{POS} infants also reflects a reduction in long-distance connectivity. The reductions in nodal local and nodal global efficiency in the HR^{POS} infants are thus not simply indices of under-connectivity, but also reflect a more random configuration with more limited local connectivity and less direct connections to other brain regions.

Networks with a high degree of spatially local connectivity, but with few or no long-range connections, that is, shortcuts, have high local efficiency and low global efficiency; networks with a high degree of long-range connectivity, but which lack spatially local clustering, have high global efficiency and low local efficiency. Biological systems in general, and neural networks in particular, reliably balance global efficiency with local efficiency, having strong local clustering mixed with sufficient long-range connectivity to allow rapid communication between distant nodes; these have been dubbed 'small-world' properties.^{34,36,37} The results here suggest that cortico-cortical organization is deficient in infants with significant symptoms of ASD in terms of both the long-range connectivity that provides for rapid integration of information between different brain regions, and the spatial clustering that provides for efficient processing for

subtasks. Notably, these abnormalities are predominately posterior, and in regions involved in early processing of auditory and visual stimuli, audio-visual integration, language and nonlinguistic social stimuli.

The economical 'small-world' organization of the typical human brain is refined over development.^{39,81,82} The results here might represent either delayed or aberrant development of this sort of economical organization. Further research is needed to determine the developmental nature of the network inefficiencies in infants who go on to a diagnosis of ASD and how these inefficiencies might relate to brain overgrowth and emerging symptoms.^{83,84} The key to understanding development is development itself.²⁷ Longitudinal data spanning infancy and toddlerhood will be essential in addressing these questions, as will four-dimensional multimodal methods to accurately estimate and analyze changes in connection lengths, connection strengths, network organization and behavior.

CONFLICT OF INTEREST

The authors declare no conflict of interest.

ACKNOWLEDGMENTS

This work was supported by a NIH Autism Center of Excellence grant (a longitudinal MRI study of infants at risk for autism, NIH, R01 Supplement, 2009–2013, NIMH and NICHD #HD055741 to Principal Investigator JP) and funding from Autism Speaks, the Simons Foundation, the Canada Foundation for Innovation (CFI), the Government of Québec, the National Science and Engineering Research Council (NSERC) and the Fonds Québécois de Recherche sur la Nature et les Technologies (FQRNT).

REFERENCES

- American Psychiatric Association. *Diagnostic and Statistical Manual of Mental Disorders*. 5th edn. American Psychiatric Publishing: Arlington, VA, USA, 2013.
- Frazier T, Hardan A. A meta-analysis of the corpus callosum in autism. *Biol Psychiatry* 2009; **66**: 935–941.
- Uddin LQ, Menon V. The anterior insula in autism: under-connected and under-examined. *Neurosci Biobehav Rev* 2009; **33**: 1198–1203.
- Just MA, Cherkassky VL, Keller TA, Minshew NJ. Cortical activation and synchronization during sentence comprehension in high-functioning autism: evidence of underconnectivity. *Brain* 2004; **127**: 1811–1821.
- Keller TA, Kana RK, Just MA. A developmental study of the structural integrity of white matter in autism. *Neuroreport* 2007; **18**: 23–27.
- Koshino H, Carpeter PA, Minshew NJ, Cherkassky VL, Keller TA, Just MA. Functional connectivity in an fMRI working memory task in high-functioning autism. *Neuroimage* 2005; **24**: 810–821.
- Just MA, Cherkassky VL, Keller TA, Kana RK, Minshew NJ. Functional and anatomical cortical underconnectivity in autism: evidence from an FMRI study of an executive function task and corpus callosum morphometry. *Cereb Cortex* 2007; **17**: 951–961.
- Murias M, Webb SJ, Greenson J, Dawson G. Resting state cortical connectivity reflected in EEG coherence in individuals with autism. *Biol Psychiatry* 2007; **62**: 270–273.
- Li H, Xue Z, Ellmore TM, Frye RE, Wong ST. Network-based analysis reveals stronger local diffusion-based connectivity and different correlations with oral language skills in brains of children with high functioning autism spectrum disorders. *Hum Brain Mapp* 2012; **35**: 396–413.
- Vissers ME, Cohen MX, Geurts HM. Brain connectivity and high functioning autism: A promising path of research that needs refined models, methodological convergence, and stronger behavioral links. *Neurosci Biobehav Rev* 2011; **36**: 604–625.
- Wilson TW, Rojas DC, Reite ML, Teale PD, Rogers SJ. Children and adolescents with autism exhibit reduced MEG steady-state gamma responses. *Biol Psychiatry* 2007; **62**: 192–197.
- Bartfeld P, Wicker B, Cukier S, Navarta S, Lew S, Sigman M. A big-world network in ASD: dynamical connectivity analysis reflects a deficit in long-range connections and an excess of short-range connections. *Neuropsychologia* 2011; **49**: 254–263.
- Belmonte MK, Allen G, Beckel-Mitchener A, Boulanger LM, Carper RA, Webb SJ. Autism and abnormal development of brain connectivity. *J Neurosci* 2004; **24**: 9228–9231.
- Noonan SK, Haist F, Müller RA. Aberrant functional connectivity in autism: evidence from low-frequency BOLD signal fluctuations. *Brain Res* 2009; **1262**: 48–63.
- Welchew DE, Ashwin C, Berkouk K, Salvador R, Suckling J, Baron-Cohen S et al. Functional disconnectivity of the medial temporal lobe in Asperger's syndrome. *Biol Psychiatry* 2005; **57**: 991–998.
- Shih P, Shen M, Öttl B, Keehn B, Gaffrey MS, Müller RA. Atypical network connectivity for imitation in autism spectrum disorder. *Neuropsychologia* 2010; **48**: 2931–2939.
- Egaas B, Courchesne E, Saitoh O. Reduced size of corpus callosum in autism. *Arch Neurol* 1995; **52**: 794–801.
- Liu Y, Cherkassky VL, Minshew NJ, Just MA. Autonomy of lower-level perception from global processing in autism: Evidence from brain activation and functional connectivity. *Neuropsychologia* 2011; **49**: 2105–2111.
- Villalobos ME, Mizuno A, Dahl BC, Kemmotsu N, Müller RA. Reduced functional connectivity between V1 and inferior frontal cortex associated with visuomotor performance in autism. *Neuroimage* 2005; **25**: 916–925.
- Turner KC, Frost L, Linsenbardt D, McIlroy JR, Müller RA. Atypically diffuse functional connectivity between caudate nuclei and cerebral cortex in autism. *Behav Brain Funct* 2006; **2**: 34.
- Courchesne E, Karns CM, Davis HR, Ziccardi R, Carper RA, Tigue ZD et al. Unusual brain growth patterns in early life in patients with autistic disorder: an MRI study. *Neurology* 2001; **57**: 245–254.
- Redcay E, Courchesne E. When is the brain enlarged in autism? A meta-analysis of all brain size reports. *Biol Psychiatry* 2005; **58**: 1–9.
- Hazlett HC, Poe M, Gerig G, Smith RG, Provenzale J, Ross A et al. Magnetic resonance imaging and head circumference study of brain size in autism: birth through age 2 years. *Arch Gen Psychiatry* 2005; **62**: 1366–1376.
- Lainhart JE, Piven J, Wzorek M, Landa R, Santangelo SL, Coon H et al. Macrocephaly in children and adults with autism. *J Am Acad Child Adolesc Psychiatry* 1997; **36**: 282–290.
- Hazlett HC, Poe MD, Gerig G, Styner M, Chappell C, Smith RG et al. Early brain overgrowth in autism associated with an increase in cortical surface area before age 2 years. *Arch Gen Psychiatry* 2011; **68**: 467–476.
- Wolff JJ, Gu H, Gerig G, Elison JT, Styner M, Gouttard S et al. Differences in white matter fiber tract development present from 6 to 24 months in infants with autism. *Am J Psychiatry* 2012; **169**: 589–600.
- Karmiloff-Smith A. Development itself is the key to understanding developmental disorders. *Trends Cogn Sci* 1998; **2**: 389–398.
- Osterling J, Dawson G. Early recognition of children with autism: a study of first birthday home videotapes. *J Autism Dev Disord* 1994; **24**: 247–257.
- Maestro S, Muratori F, Cavallaro MC, Pei F, Stern D, Golse B et al. Attentional skills during the first 6 months of age in autism spectrum disorder. *J Am Acad Child Adolesc Psychiatry* 2002; **41**: 1239–1245.
- Zwaigenbaum L, Bryson S, Rogers T, Roberts W, Brian J, Szatmari P. Behavioral manifestations of autism in the first year of life. *Int J Dev Neurosci* 2005; **23**: 143–152.
- Brian J, Bryson S, Garon N, Roberts W, Smith I, Szatmari P et al. Clinical assessment of autism in high-risk 18-month-olds. *Autism* 2008; **12**: 433–456.
- Georgiades S, Szatmari P, Zwaigenbaum L, Bryson S, Brian J, Roberts W et al. A prospective study of autistic-like traits in unaffected siblings of probands with autism spectrum disorder. *JAMA Psychiatry* 2013; **70**: 42–48.
- Messinger D, Young GS, Ozonoff S, Dobkins K, Carter A, Zwaigenbaum L et al. Beyond autism: a baby siblings research consortium study of high-risk children at three years of age. *J Am Acad Child Adolesc Psychiatry* 2013; **52**: 300–308.
- Watts DJ, Strogatz SH. Collective dynamics of 'small-world' networks. *Nature* 1998; **393**: 440–442.
- Rudie J, Brown J, Beck-Pancer D, Hernandez L, Dennis E, Thompson P et al. Altered Functional and Structural Brain Network Organization in Autism. *Neuroimage Clin* 2013; **2**: 79–94.
- Latora V, Marchiori M. Efficient behavior of small-world networks. *Phys Rev Lett* 2001; **87**: 198701.
- Latora V, Marchiori M. Economic small-world behavior in weighted networks. *Eur Phys J B* 2003; **32**: 249–263.
- Achard S, Bullmore E. Efficiency and cost of economical brain functional networks. *PLoS Comput Biol* 2007; **3**: e17.
- Bullmore E, Sporns O. The economy of brain network organization. *Nat Rev Neurosci* 2012; **13**: 336–349.
- Gotham K, Risi S, Pickles A, Lord C. The Autism Diagnostic Observation Schedule: revised algorithms for improved diagnostic validity. *J Autism Dev Disord* 2007; **37**: 613–627.
- Gotham K, Pickles A, Lord C. Standardizing ADOS scores for a measure of severity in autism spectrum disorders. *J Autism Dev Disord* 2009; **39**: 693–705.
- Gouttard S, Styner M, Prastawa M, Piven J, Gerig G. Assessment of Reliability of Multi-site Neuroimaging Via Traveling Phantom Study. In Metaxas, D, Axel, L,

- Fichtinger, G, Székely, G (eds). *Medical Image Computing and Computer-Assisted Intervention—MICCAI 2008*. Springer: Berlin/Heidelberg, 2008, vol. 5242, 263–270.
- 43 Caramanos Z, Fonov VS, Francis SJ, Narayanan S, Pike GB, Collins DL *et al*. Gradient distortions in MRI: characterizing and correcting for their effects on SIENA-generated measures of brain volume change. *Neuroimage* 2010; **49**: 1601–1611.
- 44 Liu Z, Wang Y, Gerig G, Gouttard S, Tao R, Fletcher T *et al*. Quality control of diffusion weighted images. In Proceedings of the SPIE Medical imaging 2010: advanced PACS-based imaging informatics and therapeutic applications; August 2010.
- 45 Sled J, Zijdenbos A, Evans A. A nonparametric method for automatic correction of intensity nonuniformity in MRI data. *IEEE Trans Med Imaging* 1998; **17**: 87–97.
- 46 Collins D, Neelin P, Peters T, Evans A. Automatic 3D intersubject registration of MR volumetric data in standardized Talairach space. *J Comput Assist Tomogr* 1994; **18**: 192–205.
- 47 Zijdenbos A, Forghani R, Evans A. Automatic 'pipeline' analysis of 3-D MRI data for clinical trials: application to multiple sclerosis. *IEEE Trans Med Imaging* 2002; **21**: 1280–1291.
- 48 Tohka J, Zijdenbos A, Evans A. Fast and robust parameter estimation for statistical partial volume models in brain MRI. *Neuroimage* 2004; **23**: 84–97.
- 49 Kim J, Singh V, Lee J, Lerch J, Ad-Dab'bagh Y, MacDonald D *et al*. Automated 3-D extraction and evaluation of the inner and outer cortical surfaces using a Laplacian map and partial volume effect classification. *Neuroimage* 2005; **27**: 210–221.
- 50 Lyttelton O, Boucher M, Robbins S, Evans A. An unbiased iterative group registration template for cortical surface analysis. *Neuroimage* 2007; **34**: 1535–1544.
- 51 Behrens T, Berg HJ, Jbabdi S, Rushworth M, Woolrich M. Probabilistic diffusion tractography with multiple fibre orientations: what can we gain? *Neuroimage* 2007; **34**: 144–155.
- 52 Tzourio-Mazoyer N, Landeau B, Papathanassiou D, Crivello F, Etard O, Delcroix N *et al*. Automated anatomical labeling of activations in SPM using a macroscopic anatomical parcellation of the MNI MRI single-subject brain. *Neuroimage* 2002; **15**: 273–289.
- 53 Gong G, He Y, Concha L, Lebel C, Gross DW, Evans AC *et al*. Mapping anatomical connectivity patterns of human cerebral cortex using in vivo diffusion tensor imaging tractography. *Cereb Cortex* 2009; **19**: 524–536.
- 54 Jenkinson M, Smith S. A global optimisation method for robust affine registration of brain images. *Med Image Anal* 2001; **5**: 143–156.
- 55 Behrens T, Johansen-Berg H, Woolrich M, Smith S, Wheeler-Kingshott C, Boulby P *et al*. Non-invasive mapping of connections between human thalamus and cortex using diffusion imaging. *Nat Neurosci* 2003; **6**: 750–757.
- 56 Rubinov M, Sporns O. Complex network measures of brain connectivity: uses and interpretations. *Neuroimage* 2010; **52**: 1059–1069.
- 57 Gallos LK, Makse HA, Sigman M. A small world of weak ties provides optimal global integration of self-similar modules in functional brain networks. *Proc Natl Acad Sci USA* 2012; **109**: 2825–2830.
- 58 Rutter M. Diagnosis and definition of childhood autism. *J Autism Dev Disord* 1978; **8**: 139–161.
- 59 Wetherby AM, Woods J, Allen L, Cleary J, Dickinson H, Lord C. Early indicators of autism spectrum disorders in the second year of life. *J Autism Dev Disord* 2004; **34**: 473–493.
- 60 Tager-Flusberg H. On the nature of linguistic functioning in early infantile autism. *J Autism Dev Disord* 1981; **11**: 45–56.
- 61 Schultz RT. Developmental deficits in social perception in autism: the role of the amygdala and fusiform face area. *Int J Dev Neurosci* 2005; **23**: 125–141.
- 62 Schultz RT, Gauthier I, Klin A, Fulbright RK, Anderson AW, Volkmar F *et al*. Abnormal ventral temporal cortical activity during face discrimination among individuals with autism and Asperger syndrome. *Arch Gen Psychiatry* 2000; **57**: 331–340.
- 63 Redcay E. The superior temporal sulcus performs a common function for social and speech perception: implications for the emergence of autism. *Neurosci Biobehav Rev* 2008; **32**: 123–142.
- 64 Schultz RT, Grelotti DJ, Klin A, Kleinman J, Van der Gaag C, Marois R *et al*. The role of the fusiform face area in social cognition: implications for the pathobiology of autism. *Philos Trans R Soc Lond B Biol Sci* 2003; **358**: 415–427.
- 65 Johnson MH, Griffin R, Sibira G, Halit H, Farroni T, De Haan M *et al*. The emergence of the social brain network: Evidence from typical and atypical development. *Dev Psychopathol* 2005; **17**: 599–619.
- 66 Elison JT, Paterson SJ, Wolff JJ, Reznick JS, Sasson NJ, Gu H *et al*. White matter microstructure and atypical visual orienting in 7-month-olds at risk for autism. *Am J Psychiatry* 2013; **170**: 899–908.
- 67 Elsabbagh M, Fernandes J, Jane Webb S, Dawson G, Charman T, Johnson MH. Disengagement of visual attention in infancy is associated with emerging autism in toddlerhood. *Biol Psychiatry* 2013; **74**: 189–194.
- 68 Elsabbagh M, Volein A, Holmboe K, Tucker L, Csibra G, Baron-Cohen S *et al*. Visual orienting in the early broader autism phenotype: disengagement and facilitation. *J Child Psychol Psychiatry* 2009; **50**: 637–642.
- 69 Guiraud JA, Kushnerenko E, Tomalski P, Davies K, Ribeiro H, Johnson MH *et al*. Differential habituation to repeated sounds in infants at high risk for autism. *Neuroreport* 2011; **22**: 845–849.
- 70 Guiraud JA, Tomalski P, Kushnerenko E, Ribeiro H, Davies K, Charman T *et al*. Atypical audiovisual speech integration in infants at risk for autism. *PLoS One* 2012; **7**: e36428.
- 71 Dinstei I, Pierce K, Eyley L, Solso S, Malach R, Behrmann M *et al*. Disrupted neural synchronization in toddlers with autism. *Neuron* 2011; **70**: 1218–1225.
- 72 Eyley LT, Pierce K, Courchesne E. A failure of left temporal cortex to specialize for language is an early emerging and fundamental property of autism. *Brain* 2012; **135**: 949–960.
- 73 Ohnishi T, Matsuda H, Hashimoto T, Kunihiro T, Nishikawa M, Uema T *et al*. Abnormal regional cerebral blood flow in childhood autism. *Brain* 2000; **123**: 1838–1844.
- 74 Zilbovicius M, Boddart N, Belin P, Poline J-B, Remy P, Mangin J-F *et al*. Temporal lobe dysfunction in childhood autism: a PET study. *Am J Psychiatry* 2000; **157**: 1988–1993.
- 75 Chugani HT, Da Silva E, Chugani DC. Infantile spasms: III. Prognostic implications of bipetromal hypometabolism on positron emission tomography. *Ann Neurol* 1996; **39**: 643–649.
- 76 Burroni L, Orsi A, Monti L, Hayek Y, Rocchi R, Vattimo AG. Regional cerebral blood flow in childhood autism: a SPET study with SPM evaluation. *Nucl Med Commun* 2008; **29**: 150–156.
- 77 Gendry Meresse I, Zilbovicius M, Boddart N, Robel L, Philippe A, Sfaello I *et al*. Autism severity and temporal lobe functional abnormalities. *Ann Neurol* 2005; **58**: 466–469.
- 78 McAlonan GM, Cheung V, Cheung C, Suckling J, Lam GY, Tai K *et al*. Mapping the brain in autism. A voxel-based MRI study of volumetric differences and inter-correlations in autism. *Brain* 2005; **128**: 268–276.
- 79 Courchesne E, Pierce K. Why the frontal cortex in autism might be talking only to itself: local over-connectivity but long-distance disconnection. *Curr Opin Neurobiol* 2005; **15**: 225–230.
- 80 Just MA, Keller TA, Malave VL, Kana RK, Varma S. Autism as a neural systems disorder: A theory of frontal-posterior underconnectivity. *Neurosci Biobehav Rev* 2012; **36**: 1292–1313.
- 81 Khundrakpam BS, Reid A, Brauer J, Carbonell F, Lewis J, Ameis S *et al*. Developmental changes in organization of structural brain networks. *Cereb Cortex* 2012; **23**: 2072–2085.
- 82 Fan Y, Shi F, Smith JK, Lin W, Gilmore JH, Shen D. Brain anatomical networks in early human brain development. *Neuroimage* 2011; **54**: 1862–1871.
- 83 Lewis JD, Elman JL. Growth-related neural reorganization and the autism phenotype: A test of the hypothesis that altered brain growth leads to altered connectivity. *Dev Sci* 2008; **11**: 135–155.
- 84 Lewis JD, Theilmann RJ, Townsend J, Evans AC. Network efficiency in autism spectrum disorder and its relation to brain overgrowth. *Front Hum Neurosci* 2013; **7**: 845.



This work is licensed under a Creative Commons Attribution-NonCommercial-NoDerivs 3.0 Unported License. The images or other third party material in this article are included in the article's Creative Commons license, unless indicated otherwise in the credit line; if the material is not included under the Creative Commons license, users will need to obtain permission from the license holder to reproduce the material. To view a copy of this license, visit <http://creativecommons.org/licenses/by-nc-nd/3.0/>